J. Fluid Mech. (1996), *vol.* 314, *pp.* 227–246

Instability and transitions of flow in a curved square duct: the development of two pairs of Dean vortices

By PHILIP A. J. MEES, K. NANDAKUMAR AND J. H. MASLIYAH

Department of Chemical Engineering, University of Alberta, Edmonton, Alberta, Canada T6G 2G6

(Received 3 April 1995 and in revised form 4 December 1995)

Steady developing flow of an incompressible Newtonian fluid in a curved duct of square cross-section (the Dean problem) is investigated both experimentally and numerically. This study is a continuation of the work by Bara, Nandakumar & Masliyah (1992) and is focused on flow rates between $Dn = 200$ and $Dn = 600$ ($Dn = Re/(R/a)^{1/2}$, where Re is the Reynolds number, R is the radius of curvature of the duct and a is the duct dimension; the curvature ratio, R/a, is 15.1).

Numerical simulations based on the steady three-dimensional Navier–Stokes equations predict the development of a 6-cell secondary flow pattern above a Dean number of 350. The 6-cell state consists of two large Ekman vortices and two pairs of small Dean vortices near the outer wall that result from the primary instability that is of centrifugal nature. The 6-cell flow state develops near $\theta = 80°$ and breaks down symmetrically into a 2-cell flow pattern.

The apparatus used to verify the simulations had a duct dimension of 1.27 cm and a streamwise length of 270°. At a Dean number of 453, different velocity profiles of the 6-cell flow state at $\theta = 90°$ and spanwise profiles of the streamwise velocity at every 20° were measured using a laser-Doppler anemometer. All measured velocity profiles, as well as flow visualization of secondary flow patterns, are in very good agreement with the simulations, indicating that the parabolized Navier–Stokes equations give an accurate description of the flow.

Based on the similarity with boundary layer flow over a concave wall (the Görtler problem), it is suggested that the transition to the 6-cell flow state is the result of a decreasing spanwise wavelength of the Dean vortices with increasing flow rate. A numerical stability analysis shows that the 6-cell flow state is unconditionally unstable. This is the first time that detailed experiments and simulations of the development of a 6-cell flow state are reported.

1. Introduction

Flow in curved ducts has been studied extensively since the early work by Williams, Hubbell & Finkell (1902), Eustice (1910, 1911, 1925) and Dean (1927, 1928). Most studies were focused on engineering applications like friction factor correlations (Adler 1934; Itō 1959; Van Dyke 1978; Manlapaz & Churchill 1980; Ramshankar & Sreenivasan 1988; Liu *et al.* 1994) and heat transfer (Mori & Nakayama 1965; Manlapaz & Churchill 1981). In the last decade the emphasis has shifted towards

more fundamental studies of flow development (Hille, Vehrenkamp & Schulz-Dubois 1985; Yao & Berger 1988; Bara, Nandakumar & Masliyah 1992), transitions and bifurcation phenomena (Winters 1987; Kao 1992). Excellent review articles on steady developing and fully developed flows in curved ducts are available by Berger, Talbot & Yao (1983), Nandakumar & Masliyah (1986), Itō (1987), Bara (1991) and Bara *et al.* (1992).

It can be shown (e.g. Berger *et al.* 1983) that the flow in a curved duct is characterized by two non-dimensional parameters: the curvature ratio, R_c, and the Dean number, Dn. In this study, the curvature ratio is defined as $R_c = R/a$ where R is the radius of curvature and a is the duct dimension. The Dean number is defined as $Dn = Re/R_c^{1/2}$, with the Reynolds number, $Re = \bar{v}_\theta a/\nu$. The Dean number is the ratio of the square root of the product of the inertia and centrifugal forces to the viscous force and is a measure of the magnitude of the secondary flow. In the loose coiling approximation, the curvature ratio is assumed to be large, in which case the flow is controlled only by the Dean number.

Fully developed flows in curved ducts of square cross-section were studied by Itō (1951), Cuming (1952), Cheng & Akiyama (1970), Cheng, Lin & Ou (1975, 1976), Joseph, Smith & Alder (1975) and Shantini & Nandakumar (1986) amongst others. The terms fully developed and two-dimensional will be used interchangeably.

The most complete bifurcation study of fully developed flows was conducted by Winters (1987). The primary solution in a curved square duct is a 2-cell flow state with two large counter-rotating Ekman vortices, induced by the pressure gradients along the top and bottom walls. This main branch is connected to a branch of 4-cell flows through two limit points at $Dn = 131$ and $Dn = 113$. The 4-cell solution consists of two large Ekman vortices and a pair of small counter-rotating Dean vortices near the centre of the outer wall that is the result of a centrifugal instability. This 4-cell state is unstable with respect to asymmetric disturbances only. Winters also found an isolated branch of 2-cell flows and unstable 4-cell flows at Dean numbers above 191. No unconditionally stable fully developed solutions exist for Dean numbers between 131 and 191. The location of the limit points varies very little for curvature ratios above 10, but at smaller curvature ratios the limit points move to increasingly higher Dean numbers. Bara *et al.* (1992) confirmed experimentally the existence of the 2-cell branch and the 4-cell branch up to a Dean number of 150, including the dual solution region.

Daskopoulos & Lenhoff (1989) calculated fully developed flows up to a Dean number of 350 and found four additional limit points on the isolated 2-cell branch. Three of the secondary flow patterns on these branches show six vortices.

Developing flows in curved ducts of square cross-section were studied by Ghia & Sokhey (1977), Humphrey, Taylor & Whitelaw (1977), Yee, Chilukuri & Humphrey (1980), Taylor, Whitelaw & Yianneskis (1982), Hille *et al.* (1985) and Soh (1988). Sankar, Nandakumar & Masliyah (1988) solved a parabolized version of the steady three-dimensional Navier–Stokes equations. For a curvature ratio of 100, they found sustained spatial oscillations to develop above $Dn = 125$, in the region where no stable two-dimensional solutions exist. These spatial oscillations were recently observed by Mees, Nandakumar & Masliyah (1996) in a curved square duct that spirals inwards.

The most complete study of developing flow in a curved square duct for Dean numbers up to 150 was performed by Bara *et al.* (1992). They investigated both experimentally and numerically the flow in a 270° curved square duct with a curvature ratio of 15.1. Velocity measurements of the developing flow at Dean numbers of 125, 137 and 150 were in good agreement with simulations using the code by Sankar *et al.* (1988).

This study is a continuation of the work by Bara *et al.* and investigates the flow development for flow rates up to $Dn = 600$, using the same apparatus as was used by Bara *et al.* Detailed velocity measurements are compared with simulations based on the code by Sankar *et al.* The emphasis of this work is on a new 6-cell flow state that develops above a Dean number of 350.

2. Governing equations

The curved square duct geometry used in this study is most conveniently described by a cylindrical coordinate system, shown in figure 1: r', θ and z' are the radial, streamwise and spanwise coordinates respectively. The duct walls are located at $z' = \pm a/2$ and $x' = \pm a/2$, where $x' = r' - R$. The flow perpendicular to the streamwise direction, in a plane containing the radial and spanwise components, is called the secondary flow.

The computer code used to track the spatial flow development solves a parabolized version of the three-dimensional, stationary Navier–Stokes equations and does not adopt the loose coiling approximation. This code was developed by Sankar *et al.* (1988) and was modified to include the option to impose symmetry along $z' = 0$. The streamwise momentum diffusion terms in the full three-dimensional steady-state Navier–Stokes equations were neglected, allowing for a simple marching-step method, rather than a global, elliptic solution method.

The non-dimensional parabolized Navier–Stokes equations for steady incompressible Newtonian flow are

$$\frac{1}{r}\frac{\partial}{\partial r}(rv_r) + \frac{1}{r}\frac{\partial v_\theta}{\partial \theta} + \frac{\partial v_z}{\partial z} = 0, \tag{2.1}$$

$$v_r\frac{\partial v_r}{\partial r} + \frac{v_\theta}{r}\frac{\partial v_r}{\partial \theta} - \frac{v_\theta^2}{r} + v_z\frac{\partial v_r}{\partial z} = -\frac{\partial p}{\partial r} + \frac{1}{Re}\left[\frac{\partial}{\partial r}\left(\frac{1}{r}\frac{\partial}{\partial r}(rv_r)\right) - \frac{2}{r^2}\frac{\partial v_\theta}{\partial \theta} + \frac{\partial^2 v_r}{\partial z^2}\right], \tag{2.2}$$

$$v_r\frac{\partial v_\theta}{\partial r} + \frac{v_\theta}{r}\frac{\partial v_\theta}{\partial \theta} + \frac{v_r v_\theta}{r} + v_z\frac{\partial v_\theta}{\partial z} = -\frac{1}{r}\frac{\partial p}{\partial \theta} + \frac{1}{Re}\left[\frac{\partial}{\partial r}\left(\frac{1}{r}\frac{\partial}{\partial r}(rv_\theta)\right) + \frac{\partial^2 v_\theta}{\partial z^2}\right], \tag{2.3}$$

$$v_r\frac{\partial v_z}{\partial r} + \frac{v_\theta}{r}\frac{\partial v_z}{\partial \theta} + v_z\frac{\partial v_z}{\partial z} = -\frac{\partial p}{\partial z} + \frac{1}{Re}\left[\frac{1}{r}\frac{\partial}{\partial r}\left(r\frac{\partial v_z}{\partial r}\right) + \frac{\partial^2 v_z}{\partial z^2}\right]. \tag{2.4}$$

Global continuity requires that

$$\int_{z=-0.5}^{z=0.5}\int_{r=R_c-0.5}^{r=R_c+0.5} v_\theta \mathrm{d}r\mathrm{d}z = 1.0. \tag{2.5}$$

The variables have been non-dimensionalized as follows:

$$r = \frac{r'}{a} = R_c + x, \quad x = \frac{x'}{a}, \quad z = \frac{z'}{a}, \quad R_c = \frac{R}{a}, \quad \boldsymbol{v} = \frac{\boldsymbol{v}'}{\overline{v'_\theta}}, \quad p = \frac{p'}{\rho\overline{v'_\theta}^2}, \quad Re = \frac{\rho a\overline{v'_\theta}}{\mu},$$

where the prime denotes dimensional quantities.

The simulation uses a simple approximation of the analytic solution for fully developed laminar straight duct flow as inlet condition. This approximation is within 1% of the analytic solution (Shah & London 1978).

The equations were solved using the SIMPLE algorithm as outlined by Patankar (1980). Equally spaced grids were used in the (x,z)-plane, ranging in size from 51×51 to 151×151 points. Streamwise step sizes ranged from $1/4°$ for a coarse grid to $1/256°$ for the finest grid. The calculations were performed in double precision on IBM RS/6000 375 and 560 machines.

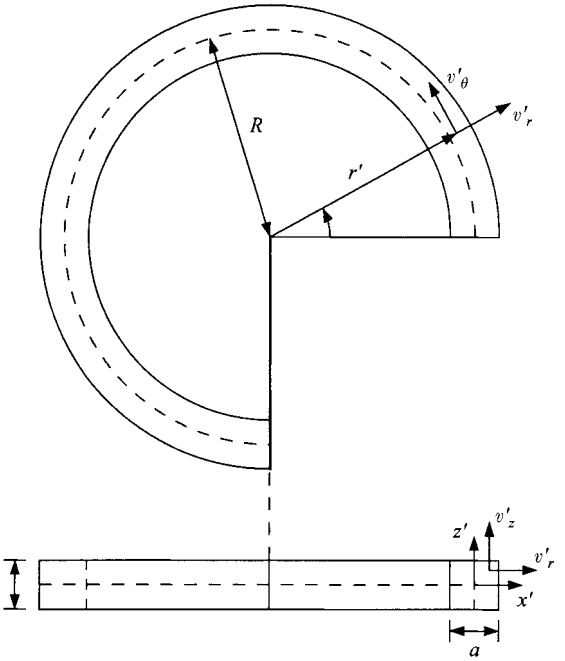

FIGURE 1. Cylindrical coordinate system.

3. Experimental setup

A schematic of the experimental setup is shown in figure 2. The curved section of the apparatus has a square cross-section of 1.27 cm and a curvature ratio, $R_c = R/a$, of 15.1. The curved duct is 270° long and is aligned in a horizontal plane. A stilling chamber and a 1 m straight inlet section were designed to provide a fully developed flow field at the inlet of the curved section for flow rates up to $Dn = 225$. A detailed description of the apparatus is given by Bara (1991) and Bara *et al.* (1992). The inlet and curved sections were made out of Plexiglas, in order to make velocity measurements and flow visualization possible. The apparatus can be rotated in a horizontal plane around the centre of curvature. This allows velocity measurements at different streamwise positions in the duct. In order to limit the buoyancy-driven secondary flows and viscosity variations, the temperature of the water was controlled to be within 23.1°C ±0.1°C.

Fluid velocities were measured with a one-component laser-Doppler anemometer that can measure either streamwise or spanwise velocities. Silicon carbide particles with a mean diameter of 1.5×10^{-6} m and a density of 3.2×10^3 kg m^{-3} were used to generate Doppler signals. The system was operated in backscatter mode, using the blue line (488 nm) of a 3 W Coherent Innova 90-3 Argon-ion laser with a typical laser power of 600 mW. Dantec 55X modular optics were used in combination with a Dantec 55N10 frequency shifter and a Dantec 55N20 Doppler frequency tracker. Dantec 57H10/57H11 traversing mechanisms provide spanwise and radial movement of the measuring volume.

Secondary flow patterns were made visible by illuminating a cross-section of the duct with a laser light sheet and injecting laser fluorescent dye at the beginning of the straight inlet section. A schematic of this setup is shown in figure 3. After the laser beam is reflected by the prism bridge, the beam either enters the LDA optics, or enters an input coupler for a 250 μm multi-mode fibre-optic ca-

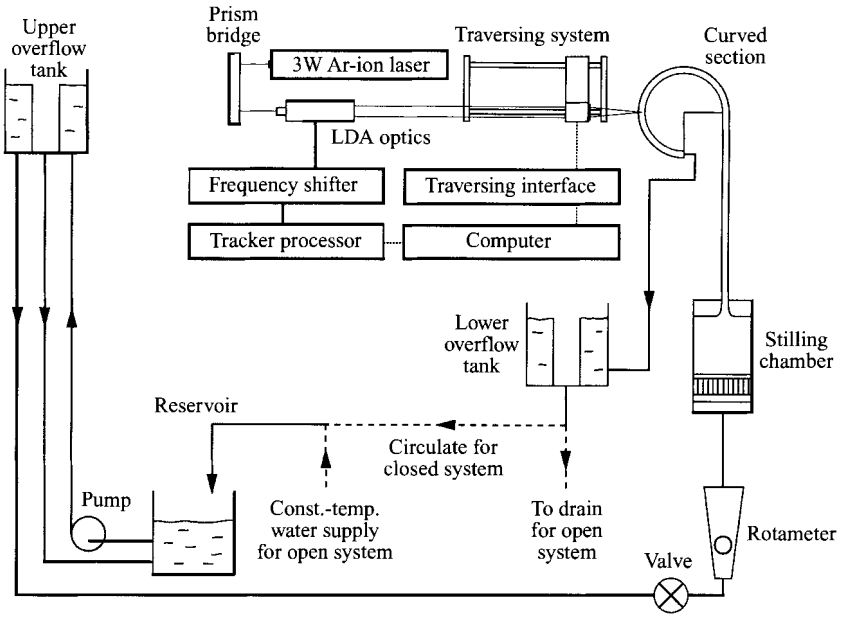

FIGURE 2. Schematic of the experimental setup.

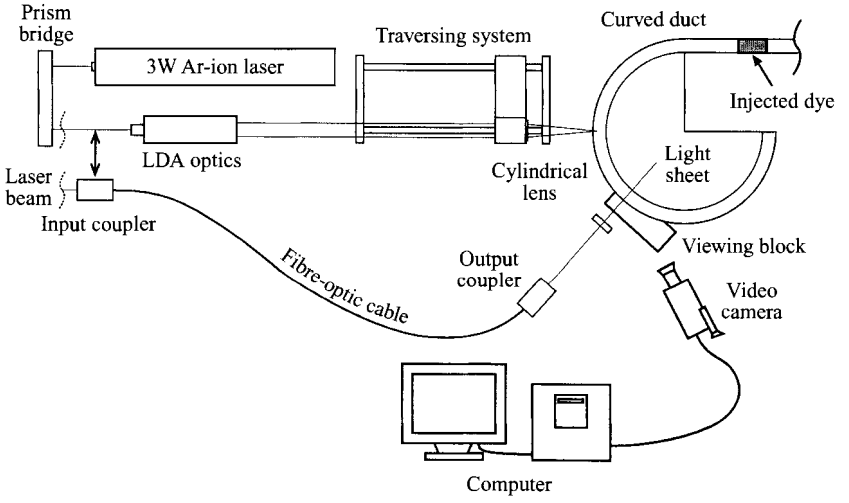

FIGURE 3. Schematic of the setup used for cross-section flow visualization.

ble. This fibre-optic cable is connected to a portable laser light sheet, created by a 10 mm focal length cylindrical lens. At the beam waist, the laser sheet is 1 mm wide and 2.5 cm long. The laser power of the sheet was typically around 500 mW. A Plexiglas viewing block, that can be positioned anywhere along the duct, corrected for some of the curvature effects. The gap between the viewing block and the duct was filled with a thin water film. Dye patterns were filmed with a Sony *CCD-V801* video camera recorder and stored on 8 mm video tape. A NeXTdimension computer was used to select, scale and enhance frames from this tape.

4. Inlet flow

Flow phenomena in open systems such as a curved duct can be very sensitive to upstream flow disturbances. Velocity fluctuations at the inlet of the curved section should therefore be kept to a minimum. Also, numerical simulations are most accurate when the experimental inlet velocity profile is used as inlet condition for the simulations. Bara (1991) showed that for Dn up to 200 the inlet flow is fully developed. In this study however, flow rates as high as $Dn = 550$ ($Re = 2138$) were used. This made it necessary to have a close look at the inlet flow conditions at these higher flow rates.

Owing to elliptic effects of the downstream curved duct flow, the velocity profile at the inlet of the curved section could deviate from fully developed straight duct flow. Humphrey *et al.* (1977) observed strong elliptic effects in a tightly curved square duct with curvature ratio 2.3. They showed numerically the presence of a 2-cell secondary flow at the inlet plane. Inlet secondary flows were about half the strength of the secondary flows at $\theta = 90°$. Bara (1991) did not expect significant elliptic effects in the large-curvature duct used in this study ($R_c = 15.1$), and this was confirmed by a simple simulation using the commercial package CFDS-FLOW3D.

Inlet velocity profiles were measured at 5 hydraulic diameters upstream of the curved section for flow rates up to $Re = 2329$ ($Dn = 599$) and compared to the analytic solution for fully developed laminar straight duct flow (Shah & London 1978). At Reynolds numbers of 397 and 774, the measured velocity profiles are within 1% of the analytic solution. At flow rates higher than $Re = 1162$ ($Dn = 300$), the difference between the measured velocity in the centre of the duct and the analytic solution increases gradually to 12% at $Re = 2329$ ($Dn = 599$). Flat regions of the velocity profiles at $Re = 1945$ ($Dn = 500$) and $Re = 2329$ ($Dn = 599$) indicate that the boundary layers have not merged yet. These results are in agreement with the experiments by Goldstein & Kreid (1967). They found that $L/a = 0.09Re$, where L is the development length. Based on this correlation, the flow in the 1 m long inlet section reaches fully developed flow up to $Re = 875$ ($Dn = 225$).

Since the highest flow rates in this study ($Re = 2329$) approached the transitional region for turbulence, the intensity of the inlet flow fluctuations was measured. The measured fluctuation intensities varied between 2% and 17% (RMS over mean) and did not contain any dominant frequencies. These measured signal fluctuations were very sensitive to the range and shift settings of the Doppler frequency tracker, suggesting that most of the signal fluctuations are the result of measurement noise. The signal fluctuations did not increase with flow rate, which indicates that the flow is in the laminar regime in the full range of flow rates. Velocities of the steady flow states presented here were measured using a low pass filter, which reduced the signal fluctuations to less than 1%.

Slow velocity fluctuations at a time scale of several minutes were an indication of a slight unsteadiness of the flow. At flow rates of $Re = 1940$ and $Re = 2330$, these slow fluctuations were between the 1% and 4%, and varied from day to day. The unsteadiness is believed to be the result of slow varying random disturbances, such as the temperature of the laboratory. Details on all aspects of the inlet flow are documented in Mees (1994).

5. Transition to 6-cell flow

Bara *et al.* (1992) calculated the flow development for a curvature ratio of 15.1 and flow rates up to $Dn = 250$, using the same parabolized Navier–Stokes equations used

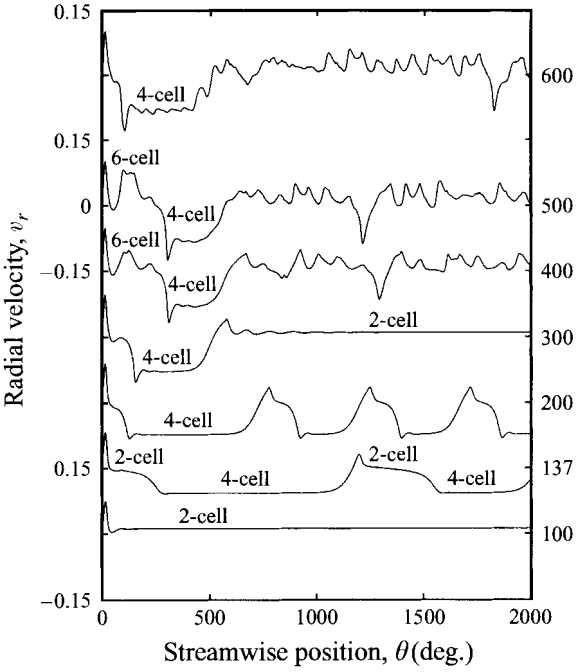

FIGURE 4. Calculated flow development diagrams of the radial velocity at $x = 0.4$, $z = 0$, showing the development to $\theta = 2000°$ at various Dean numbers.

in this study. At Dean numbers between 130 and 200, they predict the development of spatial oscillations between a 2-cell and a 4-cell state. The breakdown of the 4-cell flow is an asymmetric process, during which the Dean vortex pair alternately moves up or down along the outer wall and folds up into one of the Ekman vortices. The numerical simulation predicts these spatial oscillations to continue up to a streamwise position of at least 3000°. These spatial oscillations have been observed up to $\theta = 2340°$ in a curved square duct that spirals inwards (Mees *et al.* 1996). These results are in agreement with Winters' conclusion that for Dean numbers between 131 and 191 no stable fully developed flows exist. The flow transitions that take place for Dean numbers up to 600 are summarized in figure 4.

Our calculations show that for Dean numbers between 250 and 300 the flow develops towards a steady 2-cell flow, most likely corresponding to a stable 2-cell solution on the isolated branch calculated by Winters.

At Dean numbers between 350 and 500 the development of a 6-cell flow state, consisting of a pair of Ekman vortices and two pairs of small Dean vortices, was observed. The 6-cell pattern develops in the first 100° of the curved duct, and immediately breaks down spatially into a 2-cell state, from which a 4-cell state develops.

A 6-cell flow state with two pairs of Dean vortices was not predicted by the bifurcation studies of two-dimensional fully developed flows by Winters (1987) and Daskopoulos & Lenhoff (1989). The additional cells of the 6-cell flow states calculated by Daskopoulos and Lenhoff do not seem to form pairs of counter-rotating vortices. However, two-dimensional flows with more than one Dean vortex pair have been observed in curved rectangular ducts with aspect ratios between 8 and 30 (Finlay & Nandakumar 1990; Thangam & Hur 1990). It seems therefore likely that a 6-cell

flow state with two pairs of Dean vortices might occur as a two-dimensional solution of curved square duct flow. Based on Benjamin's view on primary mode exchange (Benjamin 1978*a*,*b*), this 6-cell flow might be stable at suitably large aspect ratios. An extensive bifurcation study for higher flow rates would have to be conducted to determine whether this 6-cell flow corresponds to a fully developed state or not and how it unfolds with changing aspect ratio. It will be shown later that if this two-dimensional 6-cell flow exists in a square duct, it is unstable to arbitrary perturbations.

The development of two pairs of Dean vortices can be explained by comparing our geometry with boundary layer flow over a concave wall, the Görtler problem. In the Görtler problem the flow in the boundary layer is centrifugally unstable, which causes a transition to streamwise, counter-rotating Görtler vortices in the boundary layer. Because of the unbound nature of the flow, Görtler vortices develop continuously in the streamwise direction, until the flow breaks down into turbulence (Bippes & Görtler 1972).

The spanwise wavelength of streamwise Görtler vortices formed in the boundary layer over a concave wall is measured by the dimensionless parameter

$$\Lambda_G = \frac{v'_{\theta,\infty}\lambda_G}{\nu}\left(\frac{\lambda_G}{R}\right)^{1/2} \tag{5.1}$$

where $v'_{\theta,\infty}$ = free-stream velocity, λ_G = dimensional wavelength in the spanwise direction.

It has been shown both experimentally and numerically that wavelengths with $\Lambda_G = 210$ generally have the largest primary growth rates (e.g. Bippes 1972; Floryan & Saric 1984 and Guo & Finlay 1994). This means that the preferred dimensional wavelength is proportional to $(v'_{\theta,\infty})^{-2/3}$ so that the size of the Görtler vortices decreases with increasing flow rate. Because of the centrifugal nature of both Dean and Görtler vortices, the former can also be expected to decrease in size with increasing flow rate.

In a curved square duct the number of Dean vortices is restricted by the top and bottom walls. With increasing flow rate, a state will be reached where two pairs of Dean vortices of the preferred wavelength can develop along the outer wall. It is conjectured that at this flow rate the transition to 6-cell flow takes place. The presence of the inner wall and especially the lateral walls of a square duct complicates the comparison between the Dean problem and the Görtler problem. It is believed however that since the mechanism that causes Dean and Görtler vortices is the same, comparison with the Görtler problem provides a qualitative explanation for the observed phenomenon.

The evolution towards a 6-cell flow has also been observed experimentally. Secondary flow patterns at $\theta = 90°$ and various flow rates are shown in figure 5. At a flow rate of $Dn = 100$ the flow develops towards a fully developed invariant 2-cell state. At $Dn = 200$ the flow develops initially into a fully developed 4-cell state, but at $\theta = 90°$ this fully developed state has not been reached yet. At $Dn = 300$ the single pair of Dean vortices that develops initially is very small and has moved down. The photograph in figure 5 for $Dn = 302.0$ shows a streak of dye at the stagnation point of this vortex pair at about $z = -0.3$ and close to the outer wall. The 6-cell secondary flow is first observed at $Dn = 350$, but the two pairs of Dean vortices are very small and break down before they can be distinguished clearly. At Dean numbers of 450 and 550 the two pairs of Dean vortices are very distinct around $\theta = 90°$, before the flow breaks down into a 2-cell state, farther downstream.

Detailed experimental observations of two pairs of Dean vortices in a curved duct of

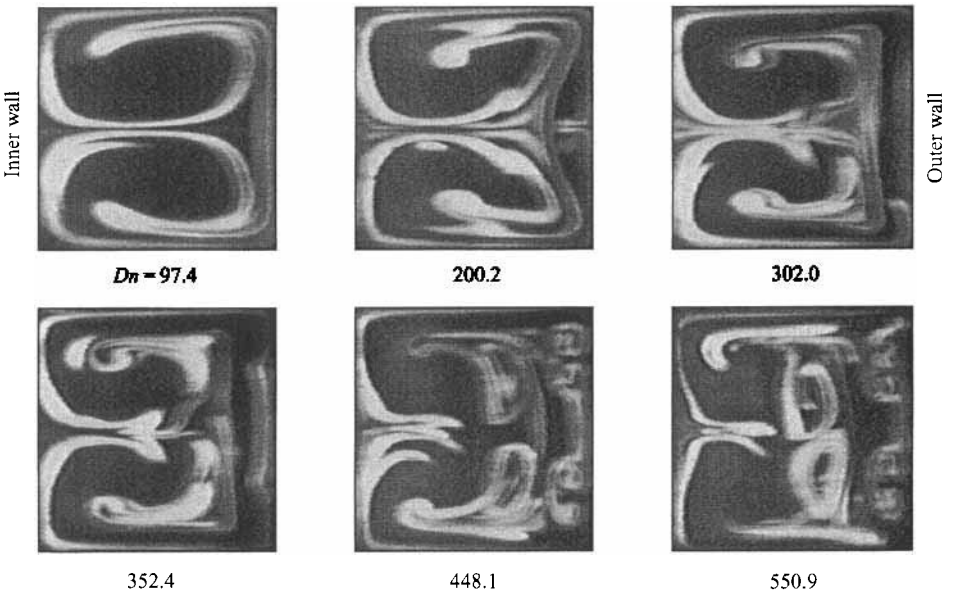

FIGURE 5. Cross-section flow visualization showing secondary flow at $\theta = 90^{\circ}$ for increasing flow rate.

square cross-section have not been reported previously. Arnal, Goering & Humphrey (1992) studied the developing flow in a curved square duct with a curvature ratio of 3.36 at a Dean number of 764. Their numerical simulations show two pairs of Dean vortices at $\theta = 135^{\circ}$, although the arrows in their figure 5 are pointing in the opposite direction. It is not clear whether they observed this 6-cell flow experimentally.

Six-cell flows have also been observed experimentally in a curved rectangular duct with an aspect ratio of 2. Sugiyama, Hayashi & Yamazaki (1983) and Sugiyama *et al.* (1988) reported detailed LDA measurements and flow visualization of the development and breakdown of 6-cell flow at a Dean number of 220 in a rectangular duct with curvature ratio 8. Numerical simulations for this geometry were performed by Miyake, Kajishima & Inaba (1988) and Kajishima, Miyake & Inaba (1989) and are in qualitative agreement with the experiments.

At a Dean number of 600, another new phenomenon is predicted by the numerical code. The flow does not develop a 6-cell pattern. Instead, a 4-cell flow is formed from the initial 2-cell flow, but no fully developed 4-cell state develops. The size and radial position of the Dean vortices keeps changing. In particular, just before the 4-cell flow breaks down (around $\theta = 400^{\circ}$), the Dean vortices oscillate strongly in the radial direction. This phenomenon was not investigated any further.

6. Flow development at $Dn = 453$

Flow visualization photographs of the flow development at a Dean number of 453 are shown in figure 6. A distinct 6-cell secondary flow pattern has developed at $\theta = 100^{\circ}$. The 6-cell flow breaks down symmetrically into a 2-cell state with one pair of Dean vortices folding up in each of the Ekman vortices. The 2-cell state that forms after the 6-cell one breaks up remains almost invariant until $\theta = 240^{\circ}$, although this is not obvious from the photographs of figure 6 because of the upstream effects on the dye pattern. A numerical study by Finlay, Guo & Olsen (1993) showed that especially

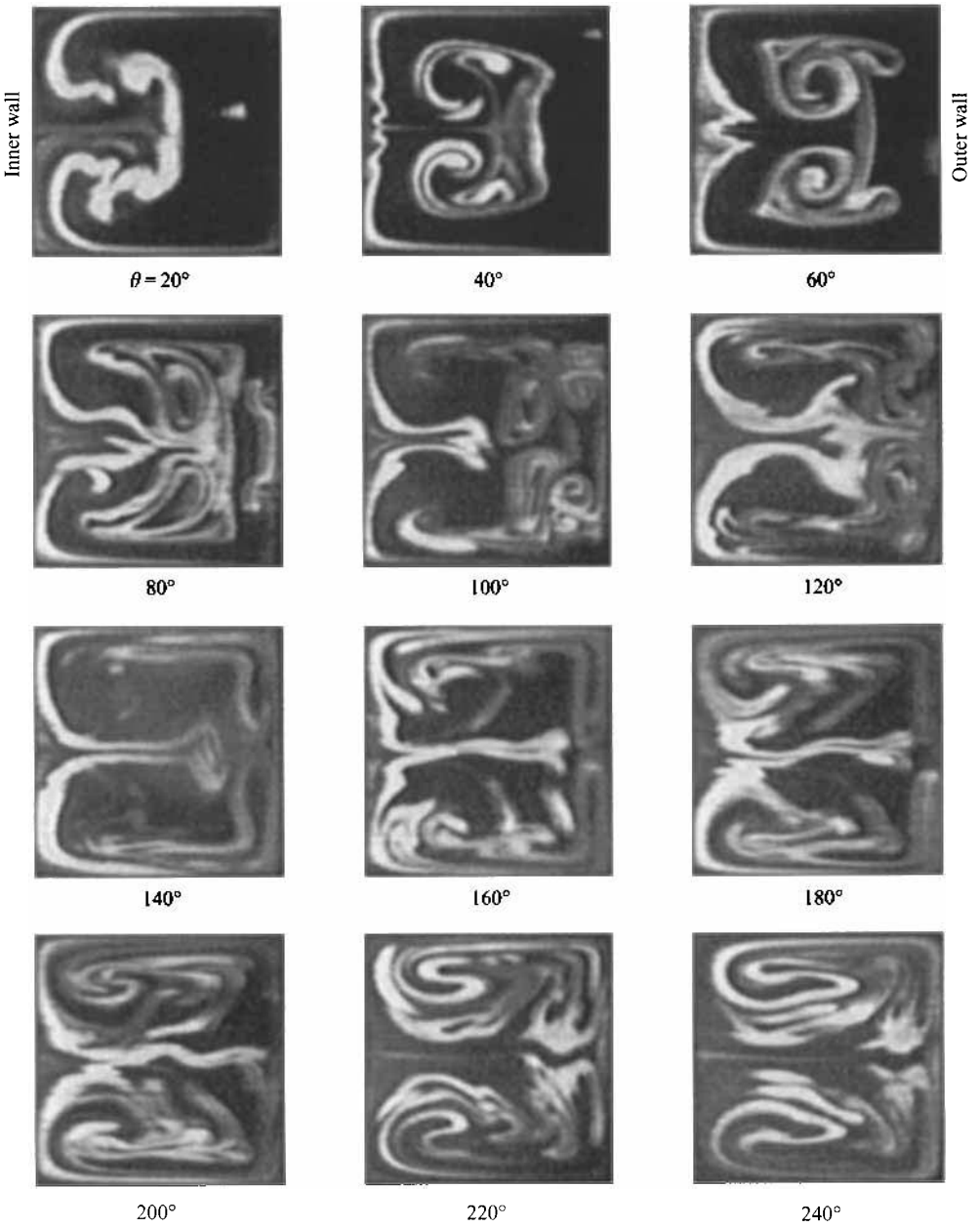

FIGURE 6. Cross-section flow visualization showing secondary flow development at $Dn = 453$.

when the flow field changes quickly in the streamwise direction, the dye pattern does not represent the local secondary flow accurately. The 2-cell state between $\theta = 140°$ and $\theta = 240°$ was confirmed by LDA measurements.

The simulated flow development diagrams of figure 7 do not show a very high grid sensitivity up to $\theta = 450°$. The simulation predicts the development of a 6-cell secondary flow around $\theta = 100°$, that breaks down into a 2-cell state. From the 2-cell state a symmetric 4-cell pattern develops around $\theta = 300°$. The flow pattern becomes

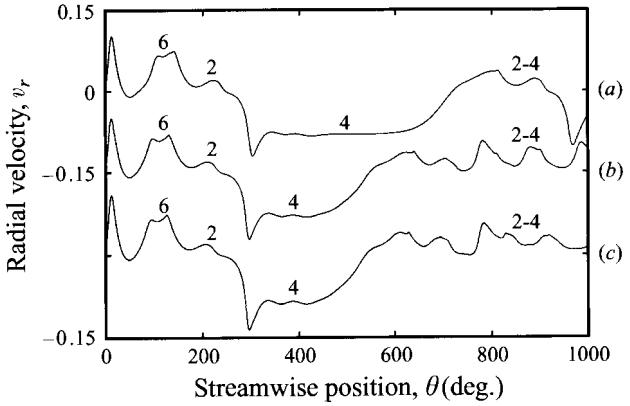

FIGURE 7. Calculated flow development diagrams of the radial velocity at $x = 0.4$, $z = 0$, showing the flow development to $\theta = 1000°$ at $Dn = 453$; $R_c = 15.1$. Labels indicate number of cells. Grid size and streamwise step size of (*a*) 51 × 51, 1/4°; (*b*) 71 × 71, 1/16°; (*c*) 101 × 101, 1/32°. The curves are offset in the vertical direction.

asymmetric when the 4-cell breaks down between $\theta = 500°$ and $\theta = 700°$, depending on the grid resolution.

Arrow plots calculated with a 101 × 101 grid are shown in figure 8 and agree very well with the experiment up to $\theta = 120°$. After that the flow visualization becomes hard to interpret.

In order to obtain a more quantitative view of the observed flow phenomena, measured velocity profiles were compared with the simulation. First the 6-cell flow at $Dn = 453$ and $\theta = 90°$ will be discussed in detail. Then a series of velocity profiles, showing the streamwise flow development, will be presented.

A surface plot of the streamwise velocity for $Dn = 453$ and $\theta = 90°$, combined with an arrow plot of the secondary flow is shown in figure 9. The two inflow regions with low streamwise velocity near the outer wall are characteristic for the 6-cell flow pattern. The inflow jets of each of the two Dean vortex pairs transfer fluid with low streamwise momentum away from the outer wall. This leads to two regions with low streamwise velocity, represented by the dents in the surface plot.

A profile of the streamwise velocity measured in the spanwise direction through the Dean vortices at $x = 0.38$ is shown in figure 10(*a*) together with the simulation result. The two minima in the profile correspond to the inflow regions near the outer wall. Although there is no perfect agreement between the experiment and the simulation, the experimental result clearly shows the presence of two Dean vortex pairs. Streamwise velocity profiles measured at $x = 0$ and $z = 0$ are shown in figures 10(*b*) and 10(*c*) and show very good agreement with the simulation results. Spanwise and radial profiles were measured at respectively 63 and 48 positions.

Careful observation of the arrow plot in figure 9 shows that the spanwise velocity along the outer wall changes direction a number of times. The experimental spanwise velocity profile at $x = 0.47$ and the simulation result are shown in figure 10(*d*). An experimental difficulty with measuring spanwise velocities is the alignment of the LDA optics. In the measured region, the streamwise velocity is more than an order of magnitude larger than the spanwise velocity. Therefore, if the alignment of the optics is off by only 1°, the contribution of the streamwise velocity to the measured signal is about 5% of the magnitude of the spanwise velocity. The error in the alignment of the LDA optics was estimated to be at least 1°. Although the margin of error is quite

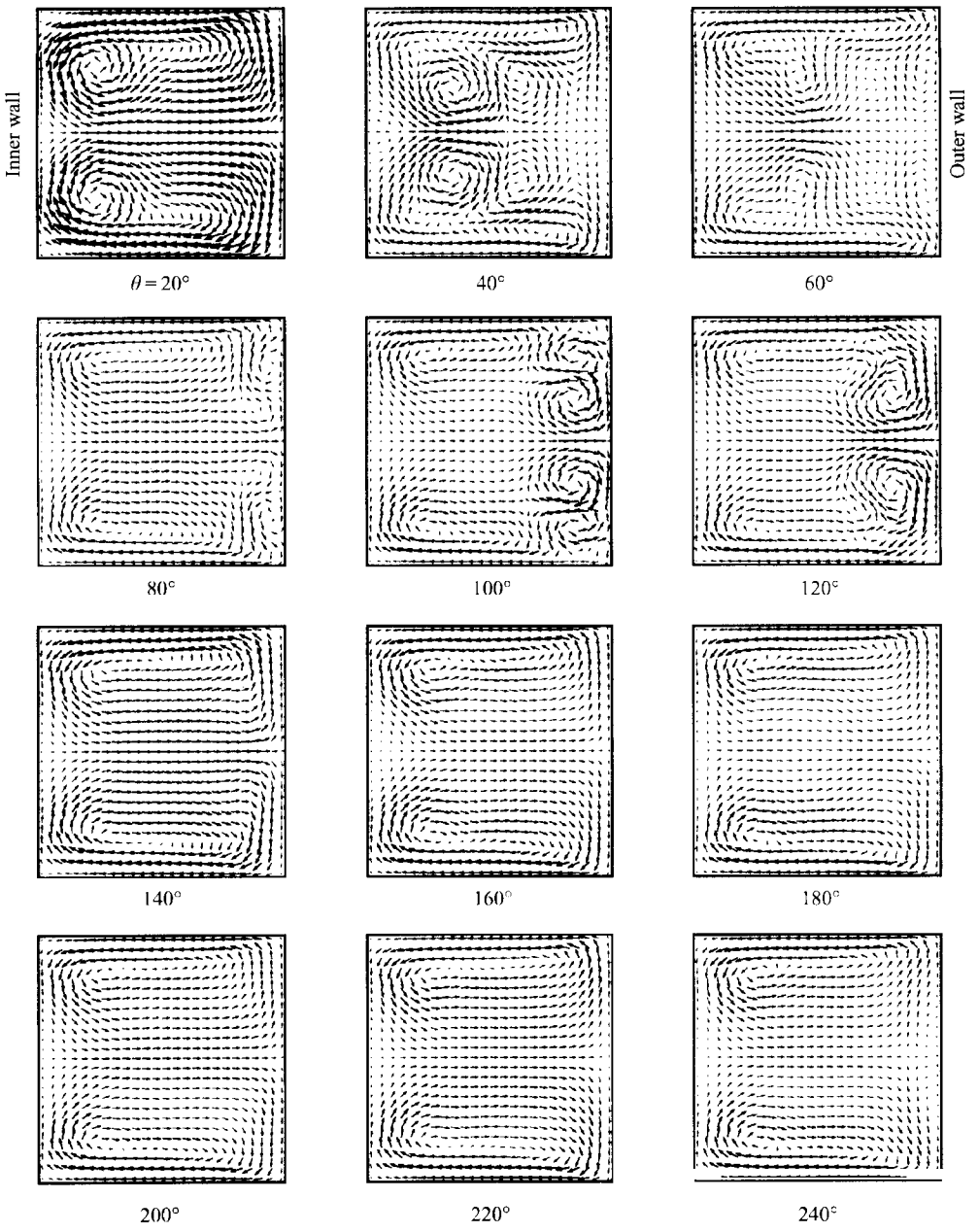

FIGURE 8. Calculated arrow plots showing secondary flow development at $Dn = 453$; $R_c = 15.1$.

high, the experimental spanwise velocity profile shows the same direction changes as the simulation.

In the simulation the most significant changes in the streamwise velocity of the developing flow take place along the outer wall. Therefore, the experimental flow development was compared to the simulation by comparing spanwise profiles of the streamwise velocity at $x = 0.38$. These profiles, taken at every 20°, are shown in figure 11. The overall agreement between the experiment and the simulation is good and shows that the model captures the physics of the flow very well.

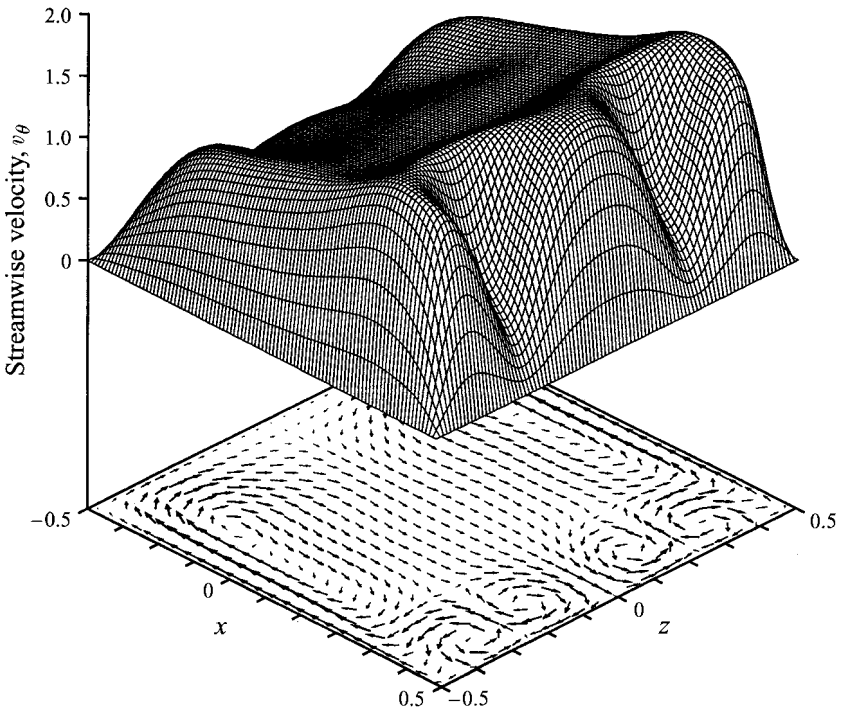

FIGURE 9. Calculated surface plot of the streamwise velocity and arrow plot showing the secondary flow at $Dn = 453$ and $\theta = 90°$; $R_c = 15.1$.

The velocity profiles at $\theta = 60°$ show the development of a wide inflow region around $z = 0$. In the arrow plot for $\theta = 60°$ in figure 8 two counter-rotating vortices have been formed along the outer wall. At lower flow rates, e.g. $Dn = 272$, this one pair of vortices reaches full development in a 4-cell secondary flow pattern. At $Dn = 453$ however, the two vortices move out towards the top and the bottom walls, while two more vortices form in the centre. As the two initial Dean vortices move apart, the single inflow region splits up into two inflow regions as shown at $\theta = 80°$. These two inflow regions keep moving towards the lateral walls as the 6-cell flow breaks up symmetrically.

The flow reaches a very distinct 6-cell flow state at $\theta = 100°$. The experimental profile is slightly asymmetric, but is in good agreement with the simulation. In the experiment the 6-cell flow has broken up into a 2-cell flow state at $\theta = 120°$. The 2-cell flow is characterized by a nearly flat velocity profile in figure 11. At $\theta = 120°$, the simulated velocity profile shows signs of Dean vortices in the form of the velocity minima near the top and bottom walls. This is the only significant discrepancy between the experiment and the model.

Downstream from $\theta = 140°$ the secondary flow is basically a 2-cell state that changes very little with the streamwise position. The velocity profiles at $x = 0.38$ and θ between 140° and 240° show a gradual change from being convex at $\theta = 140°$ to flat at $\theta = 220°$ and concave at $\theta = 240°$. All these profiles are in excellent agreement with the simulation results. The secondary flow at θ between 140° and 240° could not be determined from the flow visualization, but the measured velocity profiles confirm the development of a 2-cell secondary flow pattern. At $\theta = 240°$ a new inflow region develops along the centre of the outer wall from which a new 4-cell state is predicted to

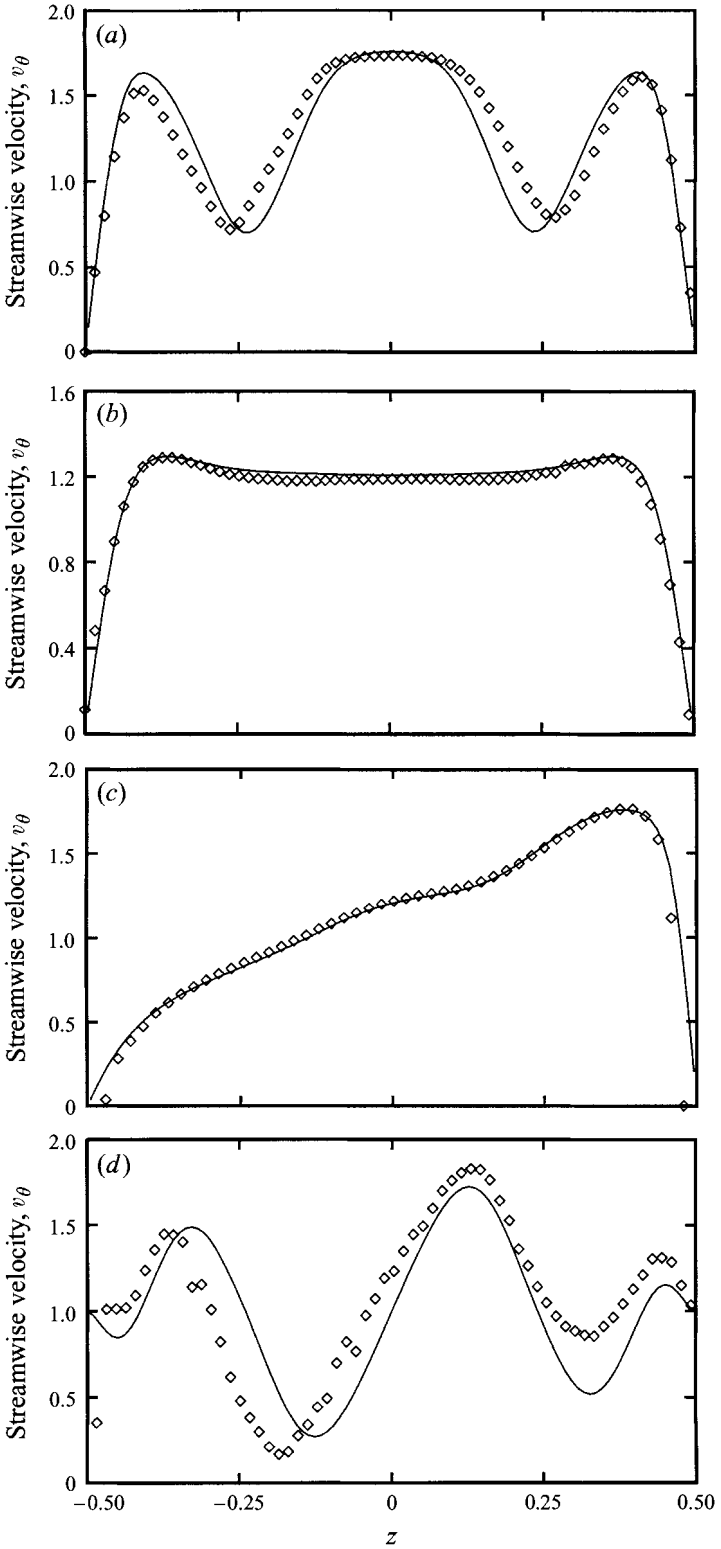

FIGURE 10. For caption see facing page.

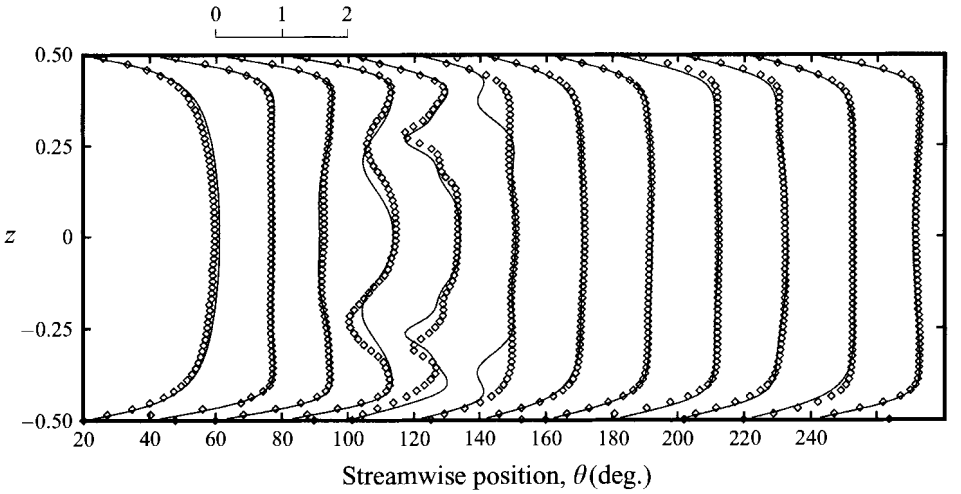

FIGURE 11. Measured spanwise profiles of the streamwise velocity compared to the simulation at $Dn = 453$ and $x = 0.38$; $R_c = 15.1$.

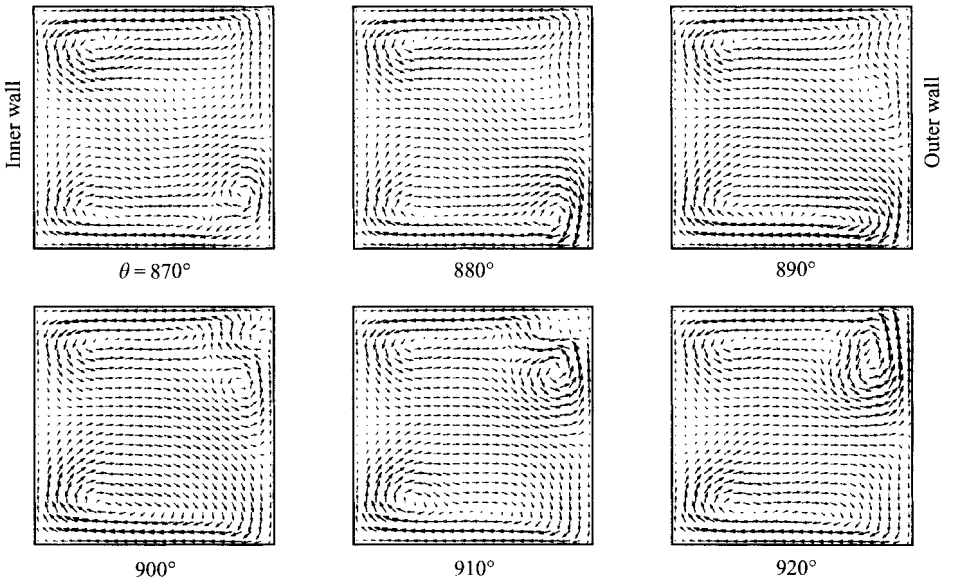

FIGURE 12. Calculated arrow plots showing randomly forming and disappearing Dean vortices at $Dn = 453$; $R_c = 15.1$.

develop (see the flow development diagram in figure 7). The simulation predicts that this 4-cell state will break down asymmetrically into a 2-cell state near $\theta = 500°$. This is the first time in the flow development that the symmetry is broken significantly.

Once the symmetric 4-cell flow has broken down at $\theta = 500°$, the simulation

FIGURE 10. (*a,b*) Measured spanwise profile of the streamwise velocity compared to the simulation at: (*a*) $x = 0.38$, (*b*) $x = 0$. (*c*) Measured radial profile of the streamwise velocity compared to the simulation at $z = 0$. (*d*) Measured spanwise profile of the spanwise velocity compared to the simulation at $x = 0.47$. $Dn = 453$, $\theta = 90°$ and $R_c = 15.1$.

predicts an unstructured kind of flow behaviour that can best be characterized as a seemingly random sequence of Dean vortex forming and breakup processes. A number of arrow plots that demonstrate this flow behaviour are shown in figure 12. Simulations on a 71×71 grid show that this random behaviour continues up to at least $\theta = 2000°$.

The development and breakup of the 6-cell flow observed here is very similar to that observed by Sugiyama *et al.* (1988) in a curved rectangular duct with an aspect ratio of 2 and a curvature ratio of 8. They measured the secondary flow in the full cross-section and used dye visualization. At a Dean number of 220 they observed the first sign of two pairs of Dean vortices at $\theta = 135°$. The 6-cell pattern is most pronounced at $\theta = 180°$ and has broken down symmetrically at $\theta = 270°$.

7. Flow stability

Two methods were used to test the stability of two-dimensional solutions, using the three-dimensional flow development code: (*a*) imposing symmetry around the horizontal centre line ($z = 0$) and (*b*) perturbing the flow asymmetrically.

By imposing symmetry around $z = 0$, asymmetries are unable to develop. Therefore, a flow state that is only unstable with respect to asymmetric perturbations is stable when symmetry is imposed. This is demonstrated in figure 13(*a*) curve(ii) for a Dean number of 300. As shown before, without symmetry the flow at $Dn = 300$ develops into a 4-cell state that breaks down asymmetrically into a stable 2-cell state (figure 13(*a*) curve(i)). Imposing symmetry makes this asymmetric fold up process impossible, and thus stabilizes the 4-cell flow.

By perturbing the flow asymmetrically at the inlet of the curved section, the initial asymmetries in the flow are increased and dominate the flow behaviour in the first stage of its development. The flow is perturbed by setting the streamwise velocity along $z = 0.06$ (3 grid points above the centreline for a 51×51 grid) to zero. Because of these strong asymmetries a symmetric 4-cell state never develops (figure 13(*a*) curve(iii)). Instead, the flow develops towards a stable 2-cell state.

A similar stability analysis was performed for a Dean number of 500. The results are shown in figure 13(*b*). Without symmetry the flow follows the familiar development of a 6-cell flow that breaks down into a 2-cell flow state from which a symmetric 4-cell develops that breaks down asymmetrically. Only when the 4-cell breaks down do asymmetries start to dominate the flow.

When symmetry is imposed the flow development is very similar up to the symmetric 4-cell state (figure 13(*b*) curve(ii)). This 4-cell state is again stabilized by the imposed symmetry. The 6-cell flow that develops around $\theta = 90°$ remains unstable. This was expected because the breakup of the 6-cell flow into a 2-cell state seems to be a symmetric process that is not hindered by imposing symmetry. This result indicates that if the 6-cell state corresponds to a fully developed solution, this 6-cell flow is unconditionally unstable.

On perturbing the flow asymmetrically, none of the symmetric flow states develop. The flow develops generally directly towards a state of randomly forming and disappearing Dean vortices, sometimes preceded by periodic spatial oscillations (figure 13(*b*) curve(iii)).

In summary, the numerical simulations support Winters' result that the symmetric 4-cell is unstable with respect to asymmetric perturbations only, and show that the 6-cell flow is unconditionally unstable.

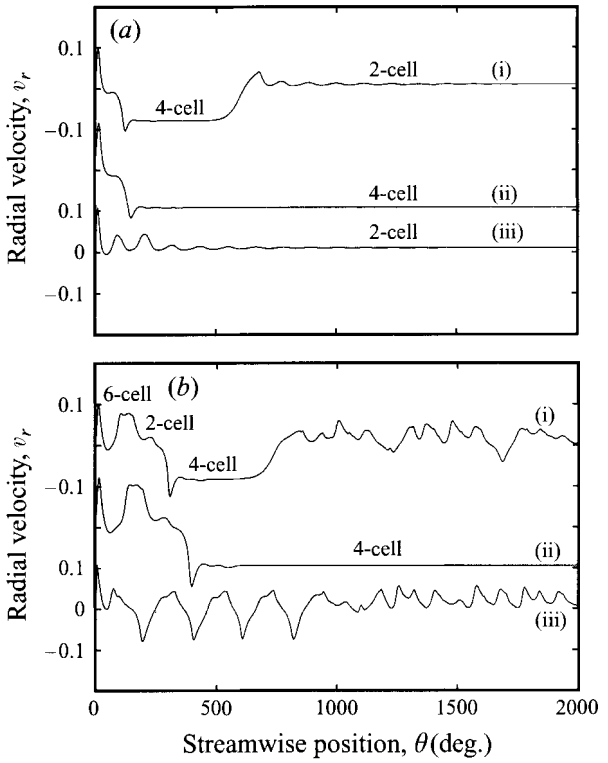

FIGURE 13. Calculated flow development diagrams of the radial velocity at $x = 0.4$, $z = 0$, showing the flow development to $\theta = 2000°$ at (*a*) $Dn = 300$, (*b*) $Dn = 500$; $R_c = 15.1$: (i) no disturbances, full domain; (ii) no disturbances, reflectional symmetry imposed at $z = 0$; (iii) flow disturbed at $\theta = 5°$, $z = 0.06$, full domain. The curves are offset in the vertical direction.

8. Summary

Experiments and numerical simulations of steady developing flow up to a Dean number of 500 ($Re = 1945$) were reported. Flow visualization and LDA measurements were used in the experiments. The simulations were based on the parabolized steady Navier–Stokes equations.

Above a Dean number of 350 a 6-cell secondary flow pattern is observed early in the flow development. A first small pair of Dean vortices splits and two new vortices are formed in between, resulting in two pairs of Dean vortices. These two vortex pairs are the result of the primary centrifugal instability. The 6-cell flow breaks down symmetrically into a 2-cell state. This process is very similar to that observed experimentally by Sugiyama *et al.* (1988) in a curved duct with aspect ratio 2. Based on the similarity with the Görtler problem, it is suggested that the transition to 6-cell flow is the result of a decreasing spanwise wavelength of the Dean vortices with increasing flow rate.

The experimental flow development at a Dean number of 453 was investigated in detail. Spanwise and radial profiles of the streamwise and spanwise velocity, as well as flow visualization of the secondary flow, are in very good agreement with the simulation. The parabolized Navier–Stokes equations capture the physics of the flow very well.

Numerical stability analyses of 4-cell and 6-cell flows were performed by imposing symmetry around the centreplane at $z = 0$ and by perturbing the inlet asymmet-

rically. It was shown that the 4-cell flow is unstable with respect to asymmetric disturbances, in agreement with Winters' calculations, and that the 6-cell flow is unconditionally unstable.

The financial support from the Natural Sciences and Engineering Research Council of Canada (NSERC) in the form of operating and equipment grants to K.N. and J.H.M., and from the University of Alberta in the form of a dissertation fellowship and the Andrew Stewart Memorial Graduate Prize to P.A.J.M. is gratefully acknowledged.

REFERENCES

ADLER, M. 1934 Strömung in gekrümmten Rohren. *Z. Angew. Math. Mech.* **14**, 257–275.

ARNAL, M. P., GOERING, D. J. & HUMPHREY, J. A. C. 1992 Unsteady laminar flow developing in a curved duct. *Intl J. Heat Fluid Flow* **13**, 347–357.

BARA, B. 1991 Experimental investigation of developing and fully developed flow in a curved duct of square cross section. PhD thesis, Department of Mechanical Engineering, University of Alberta.

BARA, B., NANDAKUMAR, K. & MASLIYAH, J. H. 1992 An experimental and numerical study of the Dean problem: flow development towards two-dimensional multiple solutions. *J. Fluid Mech.* **244**, 339–376.

BENJAMIN, T. B. 1978*a* Bifurcation phenomena in steady flows of a viscous fluid, I. Theory. *Proc. R. Soc. Lond.* A **359**, 1–26.

BENJAMIN, T. B. 1978*b* Bifurcation phenomena in steady flows of a viscous fluid, II. Eperiments. *Proc. R. Soc. Lond.* A **359**, 27–43.

BERGER, S. A., TALBOT, L. & YAO, L.-S. 1983 Flow in curved pipes. *Ann. Rev. Fluid Mech.* **15**, 461–512.

BIPPES, H. 1972 Experimentelle Untersuchung des laminar-turbulenten Umschlags an einer parallel angeströmten konkaven Wand. *Sitzungsber. Heidel. Akad. Wiss., Math.-naturwiss. Kl.* **3**, 103–180. Also *NASA Tech. Mem.* 75243 (1978).

BIPPES, H. & GÖRTLER, H. 1972 Dreidimensionale Störungen in der Grenzschicht an einer konkaven Wand. *Acta Mech.* **14**, 251–267.

CHENG, K. C. & AKIYAMA, M. 1970 Laminar forced convection heat transfer in curved rectangular channels. *Intl J. Heat Mass Transfer* **13**, 471–490.

CHENG, K. C., LIN, R.-C. & OU, J.-W. 1975 Graetz problem in curved square channels. *Trans. ASME* C: *J. Heat Transfer* **97**, 244–248.

CHENG, K. C., LIN, R.-C. & OU, J.-W. 1976 Fully developed flow in curved rectangular channels. *Trans. ASME* I: *J. Fluids Engng.* **98**, 41–48.

CUMING, H. G. 1952 The secondary flow in curved pipes. *Aeronaut. Res. Counc. Rep. Mem.* 2880.

DASKOPOULOS, P. & LENHOFF, A. M. 1989 Flow in curved ducts: bifurcation structure for stationary ducts. *J. Fluid Mech.* **203**, 125–148.

DEAN, W. R. 1927 Note on the motion of fluid in a curved pipe. *Phil. Mag.* (7) **4**, 208–223.

DEAN, W. R. 1928 The stream-line motion of fluid in a curved pipe. *Phil. Mag.* (7) **5**, 673–695.

EUSTICE, J. 1910 Flow of water in curved pipes. *Proc. R. Soc. Lond.* A **84**, 107–118.

EUSTICE, J. 1911 Experiments on stream-line motion in curved pipes. *Proc. R. Soc. Lond.* A **85**, 119–131.

EUSTICE, J. 1925 Flow of fluids in curved passages. *Engineering*, November 13, 604–605.

FINLAY, W. H., GUO, Y. & OLSEN, D. 1993 Inferring secondary flows from smoke or dye flow visualization: Two case studies. *Phys. Fluids* A **5**, 2689–2701.

FINLAY, W. H. & NANDAKUMAR, K. 1990 Onset of two-dimensional cellular flow in finite curved channels of large aspect ratio. *Phys. Fluids* A **2**, 1163–1174.

FLORYAN, J. M. & SARIC, W. S. 1984 Wavelength selection and growth of Görtler vortices. *AIAA J.* **22**, 1529–1538.

GHIA, K. N. & SOKHEY, J. S. 1977 Laminar incompressible viscous flow in curved ducts of regular cross-sections. *Trans. ASME* I: *J. Fluids Engng* **99**, 640–648.

GOLDSTEIN, R. J. & KREID, D. K. 1967 Measurement of laminar flow development in a square duct using a laser-Doppler flowmeter. *Trans. ASME* E: *J. Appl. Mech.* **34**, 813–818.

GUO, Y. & FINLAY, W. H. 1994 Wavenumber selection and irregularity of spatially developing nonlinear Dean and Görtler vortices. *J. Fluid Mech.* **264**, 1–40.

HILLE, P., VEHRENKAMP, R. & SCHULZ-DUBOIS, E. O. 1985 The development and structure of primary and secondary flow in a curved square duct. *J. Fluid Mech.* **151**, 219–241.

HUMPHREY, J. A. C, TAYLOR, A. M. K. & WHITELAW, J. H. 1977 Laminar flow in a square duct of strong curvature. *J. Fluid Mech.* **83**, 509–527.

ITŌ, H. 1951 Theory on laminar flows through curved pipes of elliptic and rectangular cross-sections. *Rep. Inst. High Speed Mech., Tōhoku Univ., Sendai, Japan* **1**, 1–16.

ITŌ, H. 1959 Friction factors for turbulent flow in curved pipes. *Trans. ASME* D: *J. Basic Engng* **81**, 123–134.

ITŌ, H. 1987 Flow in curved pipes. *JSME Intl J.* II **30**, 543–552.

JOSEPH, B., SMITH, E. P. & ALDER, R. J. 1975 Numerical treatment of laminar flow in helically coiled tubes of square cross section. Part 1. Stationary helically coiled tubes. *AIChE J.* **21**, 965–974.

KAJISHIMA, T., MIYAKE, Y. & INABA, T. 1989 Numerical simulation of laminar flow in curved ducts of rectangular cross-section. *JSME Intl J.* II **32**, 516–522.

KAO, H. C. 1992 Some aspects of bifurcation structure of laminar flow in curved ducts. *J. Fluid Mech.* **243**, 519–539.

LIU, S., AFACAN, A., NASR-EL-DIN, H. A. & MASLIYAH, J. H. 1994 An experimental study of pressure drop in helical pipes. *Proc. R. Soc. Lond.* A **444**, 307–316.

MANLAPAZ, R. L. & CHURCHILL, S. W. 1980 Fully developed laminar flow in a helically coiled tube of finite pitch. *Chem. Engng Commun.* **7**, 57–78.

MANLAPAZ, R. L. & CHURCHILL, S. W. 1981 Fully developed laminar convection from a helical coil. *Chem. Engng Commun.* **9**, 185–200.

MEES, P. A. J. 1994 Instability and transitions of flow in a curved duct of square cross section. PhD thesis, Department of Chemical Engineering, University of Alberta.

MEES, P. A. J., NANDAKUMAR, K. & MASLIYAH, J. H. 1996 Steady spatial oscillations in a curved duct of square cross section (submitted for publication).

MIYAKE, Y., KAJISHIMA, T. & INABA, T. 1988 Numerical experiment of laminar flow in curved ducts of rectangular cross-section. In *Experimental Heat Transfer, Fluid Mechanics, and Thermodynamics: Proc. First World Conf. on Experimental Heat Transfer, Fluid Mechanics, and Thermodynamics, Sept. 4-9, Dubrovnik, Yugoslavia* (ed. R. K. Shah, E. N. Ganić & K. T. Yand), pp. 1192–1199.

MORI, Y. & NAKAYAMA, W. 1965 Study on forced convective heat transfer in curved pipes. Part 1. *Intl J. Heat Mass Transfer* **8**, 67–82.

NANDAKUMAR, K. & MASLIYAH, J. H. 1986 Swirling flow and heat transfer in coiled and twisted pipes. In *Advances in Transport Processe* (ed. A. S. Mujumdar & R. A. Mashelkar), pp. 49–112. New Delhi: Wiley Eastern.

PATANKAR, S. V. 1980 *Numerical Heat Transfer and Fluid Flow.* Washington, DC: Hemisphere.

RAMSHANKAR, R. & SREENIVASAN, K. R. 1988 A paradox concerning the extended Stokes series solution for the pressure drop in coiled pipes. *Phys. Fluids* **31**, 1339–1347.

SANKAR, S. R., NANDAKUMAR, K. & MASLIYAH, J. H. 1988 Oscillatory flows in coiled square ducts. *Phys. Fluids* **31**, 1348–1359.

SHAH, R. K. & LONDON, A. L. 1978 *Laminar Flow Forced Convection in Ducts.* Academic.

SHANTINI, W. & NANDAKUMAR, K. 1986 Bifurcation phenomena of generalized newtonian fluids in curved rectangular ducts. *J. Non-Newtonian Fluid Mech.* **22**, 35–60.

SOH, W. Y. 1988 Developing fluid flow in a curved duct of square cross-section and its fully developed dual solutions. *J. Fluid Mech.* **188**, 337–361.

SUGIYAMA, S., AOI, T., YAMAMOTO, M., NARISAWA, N. & MIYAKE, Y. 1988 Measurements on developing laminar flow in a curved rectangular duct by means of LDV. In *Experimental Heat Transfer, Fluid Mechanics, and Thermodynamics: Proc. First World Conf. on Experimental Heat Transfer, Fluid Mechanics, and Thermodynamics, Sept. 4-9, Dubrovnik, Yugoslavia* (ed. R. K. Shah, E. N. Ganić, & K. T. Yang), pp. 1185–1191.

SUGIYAMA, S., HAYASHI, T. & YAMAZAKI, K. 1983 Flow characteristics in the curved rectangular channels. *Bull. JSME* **26**, 964–969.

TAYLOR, A. M. K. P., WHITELAW, J. H. & YIANNESKIS, M. 1982 Curved ducts with strong secondary

motion: velocity measurements of developing laminar and turbulent flow. *Trans. ASME* I: *J. Fluids Engng* **104**, 350–359.

THANGAM, S. & HUR, N. 1990 Laminar secondary flows in curved rectangular ducts. *J. Fluid Mech.* **217**, 421–440.

VAN DYKE, M. 1978 Extended Stokes series: laminar flow through a loosely coiled pipe. *J. Fluid Mech.* **86**, 129–145.

WILLIAMS, G. S., HUBBELL, C. W. & FINKELL, G. H. 1902 Experiments at Detroit, Michigan on the effect of curvature on the flow of water in pipes. *Trans. ASCE* **47**, 1–196.

WINTERS, K. H. 1987 A bifurcation study of laminar flow in a curved tube of rectangular cross-section. *J. Fluid Mech.* **180**, 343–369.

YAO, L.-S. & BERGER, S. A. 1988 The three-dimensional boundary layer in the entry region of curved pipes with finite curvature ratio. *Phys. Fluids* **31**, 486–494.

YEE, G., CHILUKURI, R. & HUMPHREY, J. A. C. 1980 Developing flow and heat transfer in strongly curved ducts of rectangular cross section. *Trans. ASME* C: *J. Heat Transfer* **102**, 285–291.